RESEARCH ARTICLE

Mechanisms of Indomethacin-Induced Alterations in the Choline Phospholipid Metabolism of Breast Cancer Cells[1]

Kristine Glunde*, Chunfa Jie[†] and Zaver M. Bhujwalla*

*MR Oncology Section, Division of MR Research, The Russell H. Morgan Department of Radiology and Radiological Science, Johns Hopkins University School of Medicine, Baltimore, MD 21205, USA; [†]McKusick-Nathans Institute for Genetic Medicine, Johns Hopkins University School of Medicine, Baltimore, MD 21205, USA

Abstract

Human mammary epithelial cells (HMECs) exhibit an increase in phosphocholine (PC) and total choline-containing compounds, as well as a switch from high glycerophosphocholine (GPC)/low PC to low GPC/high PC, with progression to malignant phenotype. The treatment of human breast cancer cells with a non-steroidal anti-inflammatory agent, indomethacin, reverted the high PC/low GPC pattern to a low PC/high GPC pattern indicative of a less malignant phenotype, supported by decreased invasion. Here, we have characterized mechanisms underlying indomethacin-induced alterations in choline membrane metabolism in malignant breast cancer cells and nonmalignant HMECs labeled with [1,2-^{13}C]choline using ^{1}H and ^{13}C magnetic resonance spectroscopy. Microarray gene expression analysis was performed to understand the molecular mechanisms underlying these changes. In breast cancer cells, indomethacin treatment activated phospholipases that, combined with an increased choline phospholipid biosynthesis, led to increased GPC and decreased PC levels. However, in nonmalignant HMECs, activation of the anabolic pathway alone was detected following indomethacin treatment. Following indomethacin treatment in breast cancer cells, several candidate genes, such as *interleukin 8*, *NGFB*, *CSF2*, *RHOB*, *EDN1*, and *JUNB*, were differentially expressed, which may have contributed to changes in choline metabolism through secondary effects or signaling cascades leading to changes in enzyme activity.

Neoplasia (2006) **8,** 758–771

Introduction

Proton and ^{31}P magnetic resonance spectroscopy (MRS) studies have detected high levels of phosphocholine (PC), phosphoethanolamine (PE), or both in most cancers, including breast cancer, whereas low levels of these metabolites have been found in corresponding normal tissues [1]. Consistently elevated PC and PE levels were observed in human breast cancer cells in culture [2,3], with PC and total choline-containing compounds (tCho) progressively increasing with malignancy [3]. An increased malignancy of breast cancer cells also resulted in higher levels of PC relative to glycerophosphocholine (GPC), as reflected by an increased PC/GPC ratio [3]. These increased PC levels in breast cancer cells can be attributed to an increased expression and/or activity of choline kinase [4,5], phospholipase D (PLD), or phospholipase C (PLC) [5,6], and/or to increased choline transport [7]. Transfection of malignant breast cancer cells by the metastasis-suppressor gene *nm23* significantly decreased the PC/GPC ratio [8], whereas an increase in PC levels was detected in NIH 3T3 cells transfected with the mutant *ras* oncogene [9], providing further evidence of a close link between choline phospholipid metabolites and malignancy. Treatment with antimicrotubule drugs significantly increased cellular GPC levels in several breast cancer cell lines [10], as did treatment with the non-steroidal anti-inflammatory agent, indomethacin [11,12]. Indomethacin increased GPC levels and decreased PC levels in breast cancer cells and in nonmalignant human mammary epithelial cells (HMECs). These data suggest that diverse genes and drugs profoundly alter choline phospholipid metabolism and result in common endpoints of change in PC and GPC.

The increase of GPC and the decrease of PC in indomethacin treatment suggest that choline compounds may be linked to inflammatory pathways [11,12]. Brain ^{1}H MRS studies of multiple sclerosis (MS) have demonstrated that an elevated choline signal was observed in inflammatory disease states [13]. Proton MRS of neuroblastoma cells treated with cyclooxygenase (COX) inhibitors demonstrated depletion of choline compounds [14]. Indomethacin is a nonsteroidal anti-inflammatory drug (NSAID) and a nonspecific COX (EC 1.14.99.1) inhibitor. Indomethacin inhibits COX-1 and COX-2 time-dependently by

noncovalently binding to the COX active site [15]. Treatment with indomethacin reduces the invasive and metastatic behaviors of human breast cancer cells [16]. Indomethacin was also shown to reduce angiogenesis [17] and tumor growth [18].

In normal tissues, arachidonic acid, a key mediator of inflammation, is released from membrane phosphatidylcholine (PtdCho) by phospholipase A_2 (PLA$_2$) (Figure 1) in response to tissue injury. Two isoforms of COX, COX-1 and COX-2, catalyze the conversion of arachidonate to prostaglandin endoperoxide H_2 (PGH$_2$) in a two-step reaction: by acting as a COX and then by exhibiting peroxidase activity. PGH$_2$ is used as an immediate substrate for a series of cell-specific prostaglandin and thromboxane synthases, which eventually synthesize different eicosanoids [19,20]. The constitutive form of COX, COX-1, is significantly overexpressed in malignant *versus* nonmalignant HMECs [11]. The inducible form of COX, COX-2, which is regulated by cytokines, growth factors, tumor promoters, and hypoxia, was shown to have high expression levels in a wide variety of human and animal tumors [21]. Increasing evidence suggests that COX-2 overexpression is caused by disturbances of cellular signaling cascades, such as the Ras−Raf−MAPkinase cascade, due to oncogenic gene mutations [21].

Recently, it was shown that the effect of indomethacin on choline metabolite profile in HMECs may be partly mediated through the upregulation of the metastasis-suppressor gene *nm23* [11]. Previous studies have demonstrated the utility of [1,2-13C]choline, in combination with 13C MRS, to the study of choline metabolism [5,22]. In this study, the 1H and 13C MRS of HMECs labeled with [1,2-13C]choline was performed to further understand the mechanisms underlying the increase of GPC relative to PC, following treatment with indomethacin in breast cancer cells and HMECs. The spontaneously immortalized nonmalignant HMEC line MCF-12A was compared with the estrogen receptor−negative, highly invasive, and metastatic human breast cancer line MDA-MB-231. Long-term and short-term incubations with [1,2-13C]choline were performed to distinguish between the anabolic and catabolic pathways of choline metabolism, as previously described [5]. A microarray-based gene expression analysis with the Human Genome U133 Set (Affymetrix, Inc., Santa Clara, CA) was performed to probe more than 39,000 transcripts derived from approximately 33,000 well-substantiated human genes [5]. This microarray analysis using the Affymetrix set was used to determine changes in gene expression profiles between control and indomethacin-treated MCF-12A HMECs and MDA-MB-231 breast cancer cells.

Methods

Cell Lines

The spontaneously immortalized nonmalignant HMEC line MCF-12A, established from MCF-12M mortal cells [23],
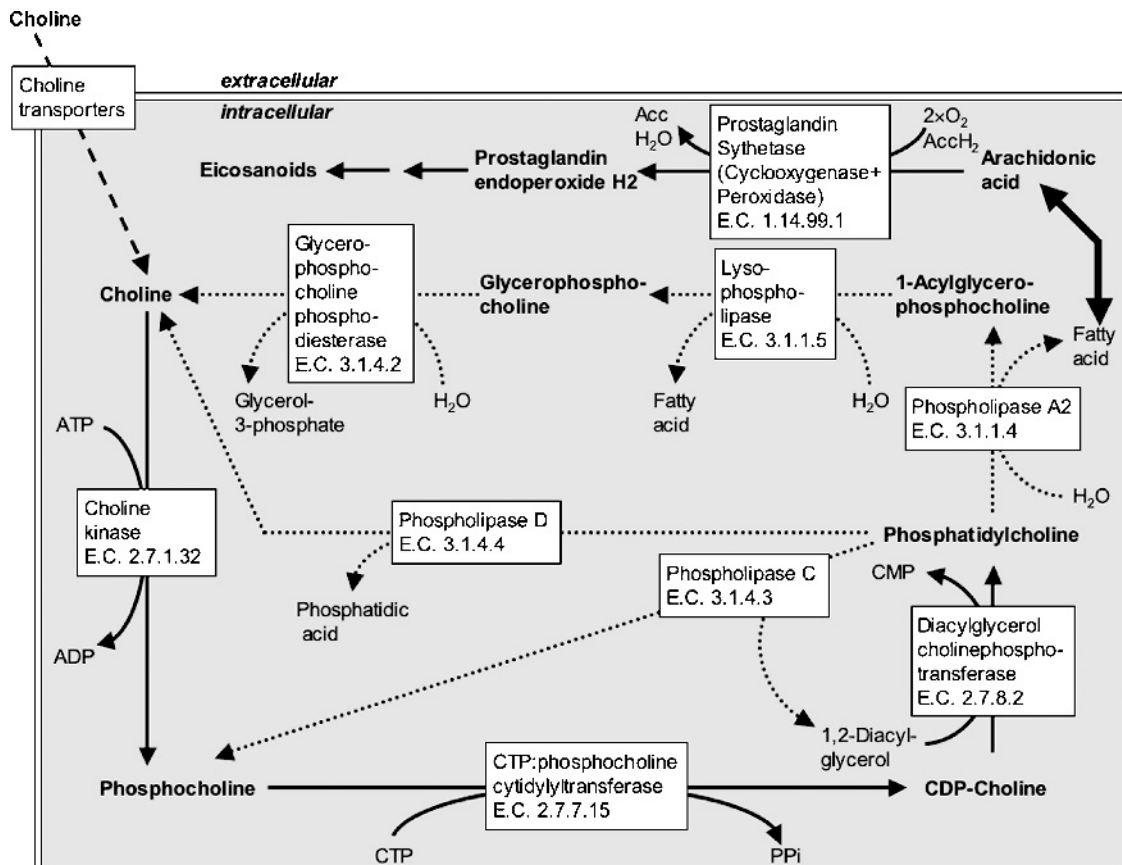

Figure 1. *Biosynthetic (solid lines) and catabolic (dashed lines) enzymatic reactions in PtdCho and arachidonic acid metabolism. CDP, cytosine diphosphate; CMP, cytosine monophosphate; CTP, cytosine triphosphate; PPi, pyrophosphate.*

was obtained from the American Type Culture Collection (Rockville, MD) and was cultured in DMEM−Ham's F12 medium (Invitrogen Corporation, Carlsbad, CA), supplemented as described previously [5,23]. The invasive and metastatic human mammary epithelial cancer cell line MDA-MB-231 was provided by Dr. R. J. Gillies (Arizona Health Sciences Center, Tucson, AZ) and was maintained in RPMI 1640 medium (Invitrogen Corporation), supplemented with 10% fetal bovine serum, 100 U/ml penicillin, and 100 μg/ml streptomycin (Invitrogen Corporation), as previously described [5].

Incubation and Dual-Phase Extraction

MCF-12A and MDA-MB-231 cells were cultured to 60% confluency. Long-term (24 +3 hours) and short-term (3 hours) labeling experiments with 100 μM [1,2-^{13}C]choline (99% ^{13}C-enriched; Cambridge Isotope Laboratories, Inc., Andover, MA) were performed for both cell lines, as previously described [5]. This approach enabled us to distinguish between the anabolic pathway and the catabolic pathway in PtdCho metabolism because, in long-term experiments, the membrane PtdCho pool of cells became partially enriched with ^{13}C, whereas in short-term experiments, the duration of exposure to the labeled substrate was not long enough for the labeling of the PtdCho pool. As a result, cells in short-term experiments contained an unlabeled membrane PtdCho pool. For long-term experiments, cells were exposed to a fresh cell culture medium containing 100 μM [1,2-^{13}C]choline for 24 hours to build up the prelabeled PtdCho pool, followed by a 3-hour experimental incubation period. For short-term experiments, cells were incubated with a fresh medium containing 100 μM unlabeled choline for 24 hours during the prelabeling period. Following the prelabeling incubation period, we performed experimental incubations. For the indomethacin-treated group, cells were incubated with 300 μM indomethacin in a medium containing 100 μM [1,2-^{13}C]choline for 3 hours. Control cells were incubated for 3 hours with a [1,2-^{13}C]choline medium alone during the experimental incubation period. Before cells were harvested and extracted, they were washed thrice, each with 10 ml of phosphate-buffered saline. Approximately 10^8 cells were harvested, and both lipid-soluble and water-soluble cell extract fractions were obtained using a dual-phase extraction method, as previously described [5,24]. Briefly, circa 10^8 cells per extract were harvested by trypsinization, washed twice with 10 ml of saline at room temperature, and pooled into a glass centrifuge tube. Cells were counted for quantitation directly after trypsinization. Four milliliters of ice-cold methanol was added to the cells, vigorously vortexed, and kept on ice for 10 minutes. Four milliliters of chloroform was added and vigorously vortexed. Finally, 4 ml of water was added, and the sample was vortexed and left overnight at 4°C for phase separation. The samples were centrifuged for 30 minutes at 35,000g at 4°C, and phases were carefully separated. The water−methanol phase containing water-soluble cellular metabolites was treated with 10 mg of Chelex for 10 minutes on ice to remove divalent cations. Chelex beads were then removed. Methanol was removed by rotary evaporation. The remaining water phases were lyophilized and stored at −20°C. The

chloroform phase containing cellular lipids was dried in a stream of N_2 and stored under N_2 at −20°C [5].

Data Acquisition and Processing

Water-soluble samples were dissolved in 0.5 ml of D_2O (Sigma-Aldrich, St. Louis, MO) containing 0.24×10^{-6} mol of 3-(trimethylsilyl)propionic-2,2,3,3,-d$_4$ acid (TSP; Sigma-Aldrich) as an internal concentration standard (sample pH of 7.4). Lipid samples were dissolved in 0.6 ml of CDCl$_3$/CD$_3$OD (2/1, vol/vol) containing 2.17×10^{-6} mol of tetramethylsilane (TMS) as an internal concentration standard (CDCl$_3$ and CD$_3$OD were premixed with TMS by the manufacturer, Cambridge Isotope Laboratories, Inc.) [5]. High-resolution proton-decoupled ^{13}C and fully relaxed ^{1}H MR spectra of all samples were acquired on a Bruker MSL-500 spectrometer operating at 11.7 T (Bruker BioSpin Corporation, Billerica, MA), as previously described [5]. Fully relaxed ^{1}H MR spectra without saturation effects were obtained at 500 MHz using a 5-mm HX inverse probe, with flip angle = 30°, sweep width = 6000 Hz, repetition time = 12.7 seconds, block size = 32,000, and scans = 128. Composite pulse (WALTZ-16) proton-decoupled ^{13}C MR spectra were recorded at 125.7 MHz using a 10-mm BB probe, with flip angle = 30°, sweep width = 29,411 Hz, repetition time = 3 seconds, block size = 16,000 (zero filling to 32,000), and scans = 20,000 (water-soluble metabolites) or 6000 (lipids). Carbon-13 MR spectra were corrected for saturation and nuclear Overhauser effects, as previously described [5]. MR spectra were analyzed using an in-house software program, Soft Fourier Transform (P. Barker, Johns Hopkins University School of Medicine, Baltimore, MD), as previously described [5]. Proton spectra were zero-filled and Fourier-transformed, and signal integrals were measured by frequency-domain fitting in Soft Fourier Transform. Carbon-13 spectra were processed using a line broadening of 1.5 Hz (zero-filled and Fourier-transformed), and signal integrals were computed in Soft Fourier Transform. The signals of TSP (water-soluble metabolites) or TMS (lipids) served as references for chemical shift and concentration in ^{1}H MR spectra. The signal integrals of the N−(CH$_3$)$_3$ signals of free choline (Cho) at 3.209 ppm, of PC at 3.227 ppm, and of GPC at 3.236 ppm in the ^{1}H MR spectra of water-soluble metabolites, as well as the N−(CH$_3$)$_3$ signal of PtdCho at 3.22 ppm in the ^{1}H MR spectra of lipids, were determined and normalized according to cell size and number, as previously described [3,5], using the following equation:

$$[\text{metabolite}] = \frac{I_{\text{metabolite}} \times \text{standard}}{I_{\text{standard}} \times \text{cell number} \times \text{cell volume}}$$

In this equation, [metabolite] represents the intracellular concentration of the metabolite of interest (in mM); $I_{\text{metabolite}}$ represents the signal integral of the metabolite of interest divided by the number of protons; and I_{standard} represents the amount of TSP (water-soluble metabolites) or TMS (lipids) used (in mol) divided by the number of protons. The number of cells in each sample (cell number) was counted before extraction, and the cell volume values used were determined

previously for MCF-12A and MDA-MB-231 cells [3,5]. Long-term and short-term [1,2-13C]choline exposure experiments did not significantly alter the total metabolite concentrations, as quantitated from 1H MR spectra. Therefore, data from these experiments were pooled.

Carbon-13 MR spectra of water-soluble metabolites were referenced to the lactate C3 signal at 21.3 ppm. Lipid 13C MR spectra were calibrated using the solvent signal of deuterated methanol at 49.5 ppm. The corrected 13C signal integral of the $N-(CH_3)_3$ group signal at 55.0 to 55.2 ppm was used as a reference to calculate the specific 13C enrichment of Cho, PC, GPC, and PtdCho. This was possible because the corrected 13C signal integral of the $N-(CH_3)_3$ group contained only the naturally abundant 13C signal contribution of Cho + PC + GPC (water-soluble metabolites) or PtdCho (lipids). The $N-(CH_3)_3$ group signal was chosen for this purpose because it was detected in the 1H MR spectra, as well as in the 13C MR spectra. The calculation of specific fractional 13C enrichments was performed with the signals of GPC, PC, and Cho within the $O-CH_2$ region because, unlike the $N-CH_2$ region, there was no signal overlap in this region. Both signals of PtdCho were used for analysis in the lipid 13C MR spectra. Fractional 13C enrichments were calculated from corrected 13C signal integrals of Cho, PC, GPC, and $N-(CH_3)_3$ in the spectra of water-soluble metabolites, and from PtdCho and $N-(CH_3)_3$ in the lipid spectra, according to the following equation:

$$\text{fractional } ^{13}\text{C enrichment}_{\text{metabolite}}$$
$$= \frac{I_{^{13}C_{\text{metabolite}}} I_{^{1}H(N-(CH_3)_3)} \times 0.0107}{I_{^{13}C(N-(CH_3)_3)} I_{^{1}H_{\text{metabolite}}}}$$

In this equation, 13C enrichment$_{\text{metabolite}}$ represents the fractional 13C enrichment within the total pool of the metabolite of interest; $I_{^{13}C_{\text{metabolite}}}$ represents the signal integral of the metabolite of interest in the 13C MR spectrum divided by the number of carbons; $I_{^{1}H(N-(CH_3)_3)}$ represents the signal integral of the $N-(CH_3)_3$ signal of (Cho + PC + GPC) or PtdCho in the 1H MR spectrum divided by the number of protons; $I_{^{13}C(N-(CH_3)_3)}$ represents the signal integral of the naturally abundant $N-(CH_3)_3$ signal of (Cho + PC + GPC) or PtdCho at 55.0 to 55.2 ppm divided by the number of carbons; and $I_{^{1}H_{\text{metabolite}}}$ represents the signal integral of the metabolite of interest in the 1H MR spectrum divided by the number of protons [5].

RNA Isolation, GeneChip Microarray Assay, and Microarray Data Analysis

Total cellular RNA was isolated from approximately 10^7 MDA-MB-231 or MCF-12A cells after 2 hours of treatment with 300 μM indomethacin, as well as from MDA-MB-231 or MCF-12A cells incubated under control conditions for 2 hours, using the RNeasy Mini Kit (Qiagen, Inc., Valencia, CA) and QIAshredder homogenizer spin columns (Qiagen, Inc.), as previously described [5]. We chose a 2-hour indomethacin incubation period for microarray experiments because we anticipated that changes in gene expression levels

would occur at a time point slightly earlier than that of metabolic changes (where indomethacin treatment was performed for 3 hours) because gene expression changes would translate into metabolic effects later. Microarray hybridization was performed at the JHMI Microarray Core Facility (Dr. Francisco Martinez Murillo, Johns Hopkins University School of Medicine) using the Human Genome U133 Set consisting of two GeneChip arrays (Affymetrix, Inc.) and the Affymetrix GeneChip platform [5]. The Human Genome U133 GeneChip Set contains approximately 45,000 probe sets representing 39,000 transcripts. GeneChip was analyzed by fluorescence detection using the Agilent GeneArray Scanner (Agilent Technologies, Inc., Palo Alto, CA). Data acquisition was performed using the Micro Array Suite 5.0 software (Affymetrix). Experiments were performed in duplicate. To estimate gene expression signals, data analysis was conducted on the chips' cell intensity file probe signal values at the Affymetrix probe pair (perfect match probe and mismatch probe) level, using statistical techniques and the package Robust Multiarray Analysis [25]. This probe-level data processing includes a normalization procedure using quantile normalization [26] to reduce obscuring variation between microarrays, which might be introduced during the processes of sample preparation, manufacture, fluorescence labeling, hybridization, and/or scanning. Using signal intensities as estimated above, an empirical Bayes method with log-normal–normal modeling, as implemented in the *R* package *EBarrays*, was used to estimate the posterior probabilities of the differential expression of genes between indomethacin-treated and control samples [27]. The criterion of the posterior probability > .5, which means that the posterior probability is larger than chance, was used to produce differentially expressed gene lists. All computations were performed under the *R* environment.

Statistical Analysis

A two-tailed *t*-test (α = 0.05) was used to detect any significant differences between the control and the indomethacin-treated groups. Because identical results were obtained in the 1H MR spectra of long-term (*n* = 3) and short-term (*n* = 3) [1,2-13C]choline exposure, 1H MR data from these experiments were pooled to give *n* = 6. *P* < .05 was considered significant.

Results

Distinct differences in choline metabolism were detected following treatment with indomethacin. Typical 13C MR spectra following long-term (*a*) or short-term (*b*) exposure to [1,2-13C]choline and the corresponding 1H (*c*) MR spectra of the water-soluble metabolites obtained from control (*lower panel*) and indomethacin-treated (*upper panel*) MDA-MB-231 human breast cancer are displayed in Figure 2. Treatment with 300 μM indomethacin for 3 hours significantly (*P* < .01) decreased the PC/GPC ratio in both MCF-12A and MDA-MB-231 cells (Figures 2*c* and 4*a*). This decrease in the PC/GPC ratio could result from a net decrease in PC levels, combined with a net increase in GPC levels, as observed in
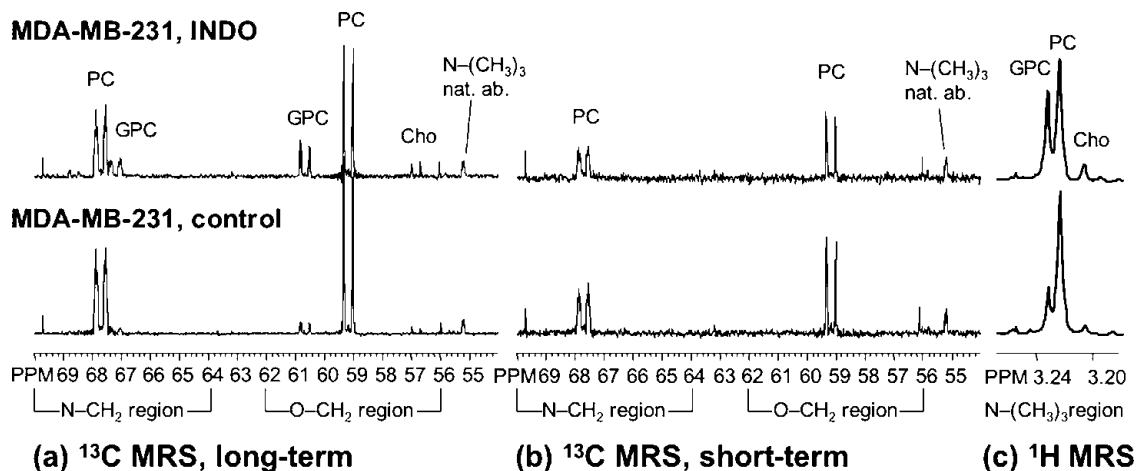
Figure 2. Representative (a) long-term ^{13}C, (b) short-term ^{13}C, and (c) ^{1}H MR spectra of the water-soluble fractions of control MDA-MB-231 breast cancer cells (bottom panel) and MDA-MB-231 cells treated with 300 μM indomethacin for 3 hours (top panel). Cells were labeled with 100 μM [1,2-^{13}C]choline for 24 + 3 hours in long-term experiments and for 3 hours in short-term experiments. MR, magnetic resonance.

the ^{1}H MR spectra of long-term and short-term experiments (Figures 2c and 4a; $n = 6$). Free cellular choline levels (Cho) significantly ($P < .05$) increased in the breast cancer cell line, but not in HMECs (Figures 2c and 4a; $n = 6$). Levels of tCho (Cho + PC + GPC) remained constant following indomethacin treatment in HMECs and breast cancer cells. ^{13}C enrichment in the GPC pool remained constant following indomethacin treatment during long-term experiments (Figures 2a and 4b; $n = 3$) in both HMECs and breast cancer cells. No ^{13}C enrichment in GPC was detected following indomethacin treatment in short-term experiments (Figure 2b) in either of the cell lines. ^{13}C enrichment of the PC pool remained relatively constant in indomethacin-treated HMECs and breast cancer cells compared to corresponding control cells in long-term experiments (Figures 2a and 4b; $n = 3$). In short-term experiments, however, ^{13}C enrichment of the PC pool significantly ($P < .05$) decreased following treatment in the breast cancer cell line, whereas it remained constant

in nonmalignant HMECs (Figures 2b and 4b; $n = 3$). The increase in Cho following indomethacin treatment in MDA-MB-231 breast cancer cells was detected in the ^{13}C MR spectra of long-term experiments (Figures 2a and 4b) and by ^{1}H MRS (Figures 2c and 4a), but not in the ^{13}C MR spectra of short-term experiments (Figures 2b and 4b). In contrast, no increased Cho levels were detected in the nonmalignant HMEC line MCF-12A following indomethacin treatment (Figure 4a). ^{13}C enrichment in the membrane PtdCho pool of long-term experiments was significantly ($P < .05$) increased following indomethacin treatment in HMECs (Figure 4b) and was slightly increased in breast cancer cells (Figures 3a and 4b). ^{13}C enrichment of the membrane PtdCho in short-term experiments was not detected in control or indomethacin-treated cells (Figure 3b).

Indomethacin treatment resulted in several changes in gene expression, which were different for MCF-12A HMECs and human MDA-MB-231 breast cancer cells, as detected by

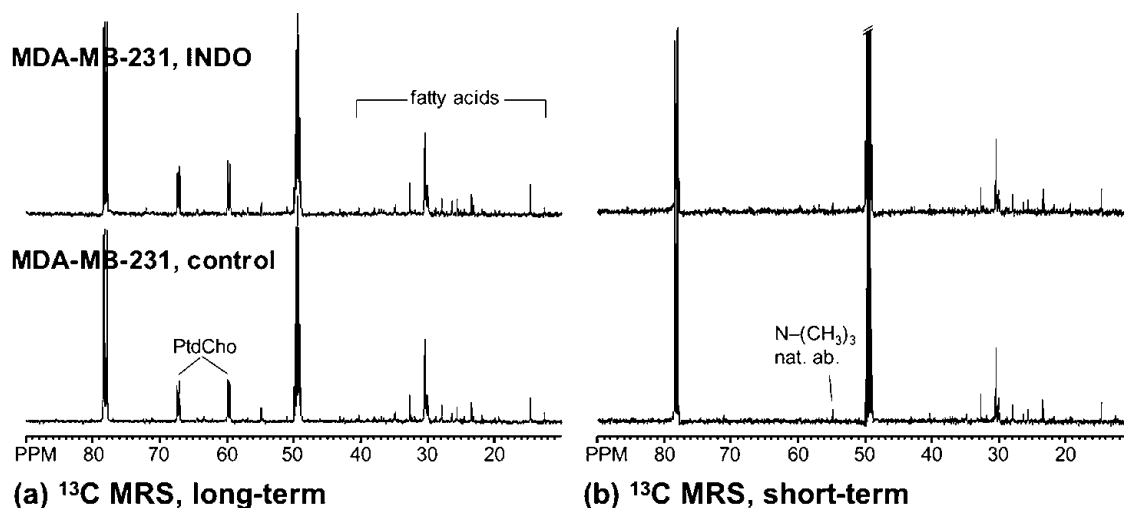**Figure 3.** Representative (a) long-term ^{13}C and (b) short-term ^{13}C MR spectra of the lipid fractions of control MDA-MB-231 breast cancer cells (bottom panel) and MDA-MB-231 cells treated with 300 μM indomethacin for 3 hours (top panel). Cells were labeled with 100 μM [1,2-^{13}C]choline for 24 + 3 hours in long-term experiments and for 3 hours in short-term experiments. MR, magnetic resonance.

(a) ¹H MR spectra [mM]
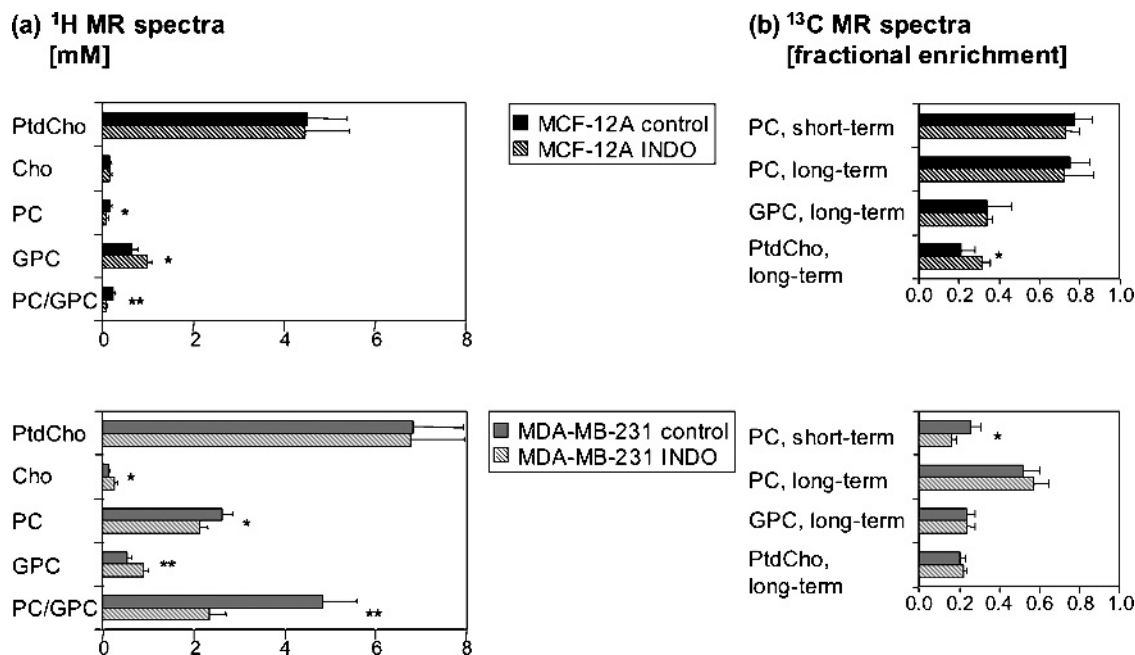

(b) ¹³C MR spectra [fractional enrichment]

Figure 4. *(a) PtdCho, Cho, PC, and GPC levels and PC/GPC ratios in indomethacin-treated MCF-12A HMECs (striped black bars) versus control MCF-12A cells (solid black bars), and indomethacin-treated MDA-MB-231 breast cancer cells (striped gray bars) versus control MDA-MB-231 cells (solid gray bars) quantified from ¹H MR spectra (n = 6). (b) Quantitation of the fractional ¹³C enrichment in PC, GPC, and PtdCho from long-term experiments (n = 3) and short-term experiments (n = 3) in indomethacin-treated (striped black bars) and control (solid black bars) MCF-12A HMECs, and indomethacin-treated (striped gray bars) and control (solid gray bars) MDA-MB-231 breast cancer cells. Cho, free choline; GPC, glycerophosphocholine; INDO, indomethacin-treated; MR, magnetic resonance; PC, phosphocholine; PtdCho, phosphatidylcholine. Values represent mean ± SD. *P < .05, **P < .01, indomethacin-treated versus control.*

mRNA analysis using Affymetrix human genome U133 A/B GeneChip combined with statistically modeled probe-level data analysis [25–27]. The Affymetrix U133 A/B GeneChip set contains all known genes of enzymes involved in choline phospholipid metabolism (Figure 1, Table 1), except the genes for GPC phosphodiesterase, which have not yet been discovered. Indomethacin significantly altered the gene expression of 151 genes in MCF-12A HMECs and of 52 genes in MDA-MB-231 breast cancer cells, using a posterior probability of > .5. No significant changes in gene expression levels of genes/proteins directly involved in choline phospholipid metabolism or choline transport, which were contained in the Affymetrix U133 A/B GeneChip set and are listed in Table 1, were detected in indomethacin-treated MCF-12A or MDA-MB-231 cells. All significantly differentially expressed genes were sorted by biologic function and are shown in Table 2 for MCF-12A HMECs and in Table 3 for human MDA-MB-231 breast cancer cells.

Genes given in the category "choline phospholipid metabolism" in Tables 2 and 3 show differentially expressed genes in MCF-12A and MDA-MB-231 cells, respectively, that can interact with choline phospholipid metabolism, but do not represent genes directly encoding enzymes in choline phospholipid metabolism. In MCF-12A HMECs, mRNA expression of protein tyrosine phosphatase nonreceptor type 12 (*PTPN12*), mitogen-activated protein kinase kinase kinase kinase 4 (*MAP4K4*), protein kinase C ι (*PRKCI*), UDP glucose ceramide glucosyltransferase (*UGCG*), and junB proto-oncogene (*JUNB*) was significantly decreased, which may

have affected choline phospholipid metabolism (Table 2). In human MDA-MB-231 breast cancer cells, interleukin (IL) 8 was significantly underexpressed, whereas *JUNB*, *ras* homolog gene family member B (*RHOB*), endothelin-1 (*EDN1*), colony-stimulating factor-2 (*CSF2*), and nerve growth factor beta (*NGFB*) polypeptide were significantly overexpressed and may have impacted on choline phospholipid metabolism (Table 3). *JUNB* was the only common choline phospholipid metabolism–related gene that was upregulated in both MCF-12A and MDA-MB-231 cells. *JUNB* overexpression was more pronounced in MDA-MB-231 breast cancer cells (3.265-fold, *P* = 1.000) compared to MCF-12A HMECs (1.578-fold, *P* = .615).

Indomethacin treatment significantly altered only seven identical genes in both MCF-12A HMECs and MDA-MB-231 breast cancer cells: *JUNB* (increase), *PLK2* (decrease), *KLF4* (increase), *TOB1* (decrease), *ANGPTL4* (increase), *PPM2C* (decrease), and *BHLHB2* (increase). The magnitudes and directions in changes in these genes were relatively comparable in MCF-12A and MDA-MB-231 cells.

Discussion

NSAIDs, such as indomethacin, are commonly used to reduce tumor-induced suppression of the immune system, to increase the effectiveness of anticancer drugs, and to improve the quality of pain control. NSAIDs also have a clear potential for use in the chemoprevention and treatment of breast cancer [28]. Indomethacin has been shown to

Table 1. Genes of Enzymes Involved in Choline Transport and Choline Phospholipid Metabolism Contained in the Affymetrix Human Genome U133 Set.

Enzyme Type	Gene Title	Gene Symbol	Representative Public ID
Choline kinase	Choline kinase alpha	*CHKA*	AI991328
	Choline kinase alpha	*CHKA*	NM_001277
	Choline kinase beta	*CHKB*	NM_005198
Diacylglycerol cholinephosphotransferase	Choline phosphotransferase 1	*CHPT1*	AF195624
Lysophospholipase	Lysophospholipase 3 (lysosomal PLA$_2$)	*LYPLA3*	AL110209
	Lysophospholipase I	*LYPLA1*	AF077198
	Lysophospholipase I	*LYPLA1*	BG288007
	Lysophospholipase II	*LYPLA2*	AK024724
	Lysophospholipase II, lysophospholipase II pseudogene 1	*LYPLA2, LYPLA2P1*	AL031295
	Lysophospholipase II, lysophospholipase II pseudogene 1 similar to acyl-protein thioesterase 2 (lysophospholipase II) (LPL-I)	*LYPLA2, LYPLA2P1, LOC388499*	NM_007260
CTP: PC cytidylyltransferase	Phosphate cytidylyltransferase 1, choline, alpha	*PCYT1A*	NM_005017
	Phosphate cytidylyltransferase 1, choline, beta	*PCYT1B*	NM_004845
	Phosphate cytidylyltransferase 1, choline, beta	*PCYT1B*	AF148464
PLA$_2$	PLA$_2$, group IB (pancreas)	*PLA2G1B*	NM_000928
	PLA$_2$, group IIA (platelets, synovial fluid)	*PLA2G2A*	NM_000300
	PLA$_2$, group IID	*PLA2G2D*	NM_012400
	PLA$_2$, group IIE	*PLA2G2E*	NM_014589
	PLA$_2$, group IIF	*PLA2G2F*	NM_022819
	PLA$_2$, group III	*PLA2G3*	NM_015715
	PLA$_2$, group IVA (cytosolic, calcium-dependent)	*PLA2G4A*	M68874
	PLA$_2$, group IVB (cytosolic)	*PLA2G4B*	NM_005090
	PLA$_2$, group IVB (cytosolic)	*PLA2G4B*	AK000550
	PLA$_2$, group IVC (cytosolic, calcium-independent)	*PLA2G4C*	AF065214
	PLA$_2$, group V	*PLA2G5*	NM_000929
	PLA$_2$, group V	*PLA2G5*	AL158172
	PLA$_2$, group V	*PLA2G5*	AL158172
	PLA$_2$, group VI (cytosolic, calcium-independent)	*PLA2G6*	NM_003560
	PLA$_2$, group VI (cytosolic, calcium-independent)	*PLA2G6*	AF102988
	PLA$_2$, group VI (cytosolic, calcium-independent)	*PLA2G6*	AK001290
	PLA$_2$, group VII (platelet-activating factor acetylhydrolase, plasma) PLA$_2$, group VII (platelet-activating factor acetylhydrolase, plasma)	*PLA2G7*	NM_005084
	PLA$_2$, group X	*PLA2G10*	NM_003561
	PLA$_2$, group XIIA, PLA$_2$, group XIIA	*PLA2G12A*	NM_030821
PLD	PLD1, phophatidylcholine-specific	*PLD1*	NM_002662
	PLD1, phophatidylcholine-specific	*PLD1*	AJ276230
	PLD1, phophatidylcholine-specific	*PLD1*	AJ276230
Choline transport	Solute carrier family 22 (extraneuronal monoamine transporter), member 3	*SLC22A3*	NM_021977
	Solute carrier family 22 (organic anion transporter), member 6	*SLC22A6*	AF124373
	Solute carrier family 22 (organic anion transporter), member 6	*SLC22A6*	AJ271205
	Solute carrier family 22 (organic anion transporter), member 7	*SLC22A7*	NM_006672
	Solute carrier family 22 (organic anion transporter), member 7	*SLC22A7*	AF210455
	Solute carrier family 22 (organic anion transporter), member 7	*SLC22A7*	AF210455
	Solute carrier family 22 (organic anion transporter), member 7	*SLC22A7*	AA777852
	Solute carrier family 22 (organic anion transporter), member 8	*SLC22A8*	NM_004254
	Solute carrier family 22 (organic anion transporter), member 8	*SLC22A8*	AW025165
	Solute carrier family 22 (organic cation transporter), member 1	*SLC22A1*	NM_003057
	Solute carrier family 22 (organic cation transporter), member 13	*SLC22A13*	NM_004256
	Solute carrier family 22 (organic cation transporter), member 14	*SLC22A14*	NM_004803
	Solute carrier family 22 (organic cation transporter), member 16	*SLC22A16*	AL050350
	Solute carrier family 22 (organic cation transporter), member 16	*SLC22A16*	AL050350
	Solute carrier family 22 (organic cation transporter), member 2	*SLC22A2*	NM_003058
	Solute carrier family 22 (organic cation transporter), member 4	*SLC22A4*	NM_003059
	Solute carrier family 22 (organic cation transporter), member 5	*SLC22A5*	NM_003060
	Solute carrier family 5 (choline transporter), member 7	*SLC5A7*	NM_021815

improve immune response [29], to prevent tumor angiogenesis [29], to enhance apoptotic cell death [30], and to reduce tumor cell invasiveness and metastases [16].

Treatment with indomethacin resulted in significantly decreased PC/GPC ratios in both nonmalignant HMECs and highly malignant human breast cancer cells, which is in excellent agreement with previously obtained results [11,12]. The decrease in the PC/GPC ratio was caused by a net decrease in PC levels and a net increase in GPC levels, as previously established [11,12]. The level of tCho, which

increases with malignant transformation [3] and is a potential diagnostic marker for breast cancer [31], was largely unaffected by indomethacin. In addition to these findings, which are consistent with our previous studies, indomethacin treatment significantly increased Cho levels in breast cancer cells but not in nonmalignant HMECs.

Short-term [1,2-^{13}C]choline exposure resulted in undetectable ^{13}C enrichment in GPC, and enrichment in GPC in long-term experiments remained constant following indomethacin treatment. Thus, the net increase in GPC following

Table 2. Significantly Differentially Expressed Genes Following Indomethacin Treatment in MCF-12A HMECs, by Function.

Function	Gene Symbol	Representative Public ID	Fold Change	Probability
Angiogenesis regulation	ANGPTL4	AF169312	1.972	1.000
	BTG1	AL535380	2.018	1.000
Apoptosis regulation	ANGPTL4	AF169312	1.972	1.000
	BTG1	AL535380	2.018	1.000
	SON	AA664291	−1.610	.885
Biosynthesis	ARG99	AU151239	−1.486	.776
	AMD1	NM_001634	−1.567	.744
	UGCG	AI378044	−1.539	.627
Cell adhesion	DST	NM_001723	−1.722	.992
	NRCAM	NM_005010	−1.584	.827
	PKP4	NM_003628	−1.584	.818
	RAPH1	AA194149	−1.475	.752
	THBS1	AW956580	−1.451	.579
Cell cycle regulation	PLK2	NM_006622	−2.783	1.000
	182-FIP	AW007746	−1.685	.999
	DST	NM_001723	−1.722	.992
	CCNG2	L49506	1.677	.985
	DNAJA2	AW057513	−1.543	.943
	CDKN1B	BC001971	−1.588	.771
	E2F3	NM_001949	−1.553	.712
Cell differentiation regulation	BTG1	AL535380	2.018	1.000
Cell growth	RBM15	NM_022768	−1.555	.654
	TMEFF2	AB004064	−1.499	.586
Cell motility	THBS1	AW956580	−1.451	.579
Choline phospholipid metabolism	PTPN12	S69182	−1.672	.985
	MAP4K4	NM_017792	−1.591	.835
	PRKCI	AI689429	−1.574	.781
	UGCG	AI378044	−1.539	.627
	JUNB	NM_002229	1.578	.615
Chromosome organization	CHD1	AU155298	−1.516	.952
Coenzyme A biosynthesis	PANK1	AI373299	−1.636	.997
Cytokinesis	ROCK2	AL049383	−1.566	.762
Cytoplasmic regulation	FUSIP1	AI954700	−1.584	.985
Cytoskeleton regulation	PRKCI	AI689429	−1.574	.781
Development	GATA6	D87811	1.559	.775
	THBS1	AW956580	−1.451	.579
Differentiation	MBNL1	BF512200	−1.610	.926
	NRCAM	NM_005010	−1.584	.827
DNA repair	REV1L	N51427	−1.455	.572
Embryonic development	MBNL1	BF512200	−1.610	.926
Exonuclease activity	FLJ12671	AW294587	−1.573	.634
Immune response	IL7	AW190593	−1.518	.878
Ion homeostasis	DKFZp434P0216	AW778829	1.491	.752
	KCTD12	AI718937	−1.638	.924
Metabolism	GLS	AI828035	−1.509	.797
	FLJ34658	AW173071	−1.461	.683
	TDG	NM_003211	−1.518	.551
Microtubule nucleation	TUBGCP3	NM_006322	−1.522	.548
Mitochondrial transport	UCP2	U94592	2.045	1.000
mRNA processing	CPSF6	AU149663	−1.490	.772
Neuron development	NRCAM	NM_005010	−1.584	.827
Not determined	PAPD5	AI492902	−1.802	1.000
	C6orf52	AW001000	1.792	1.000
	FLJ22490	AI400587	−1.724	1.000
	YTHDF3	AU157915	−1.835	1.000
	ARRDC3	AB037797	1.705	.999
	VMP1	BF674052	1.687	.999
	PDCD1LG1	AI608902	−1.655	.998
	WTAP	AU147416	−1.668	.992
	MGC14289	AI188445	−1.589	.986
	C3orf6	AV683852	−1.556	.972
	FLJ20729	NM_017953	−1.645	.962
	TXNIP	AI439556	1.697	.961
	DKFZp451J1719	AI982535	−1.547	.958
	ZC3HAV1	AI133727	−1.656	.958
	C20orf158	AW664953	−1.535	.945
	LOC124512	AA883486	1.560	.941
	YTHDF2	NM_016258	−1.610	.893
	EXOC8	AI168350	−1.505	.854
	ZCCHC7	BG291039	−1.498	.853
	ALS2CR4	AU150140	−1.491	.798
	NHSL1	AA503387	−1.490	.770

Table 2. (*continued*)

Function	Gene Symbol	Representative Public ID	Fold Change	Probability
Not determined	PHACTR2	AW880875	−1.479	.745
	KIAA0261	D87450	−1.556	.714
	HELLS	AI807356	−1.469	.677
	HSPC063	AU144305	−1.463	.675
	LOC132671	AI559300	−1.494	.662
	LOC285338	BF691831	−1.457	.638
	KIAA0143	AA805651	−1.550	.617
	KIAA0853	BE895685	−1.541	.604
	NCOA6IP	NM_024831	−1.538	.593
	AEBP2	BF475280	−1.445	.589
	FLJ20696	AI979334	−1.456	.533
	ACRBP	AI141116	1.443	.509
Nucleoside metabolism	UPP1	NM_003364	1.632	.815
Nucleotide excision repair	RAD23B	NM_002874	−1.602	.694
Proliferation regulation	KLF4	BF514079	2.771	1.000
	BTG1	AL535380	2.018	1.000
	TOB1	AA675892	−1.671	.978
	EDD	U69567	−1.640	.946
	DNAJA2	AW057513	−1.543	.943
	IL7	AW190593	−1.518	.878
	CDKN1B	BC001971	−1.588	.771
Protein biosynthesis	EIF1AX	AL079283	−1.675	.971
Protein dephosphorylation	PTPN12	S69182	−1.672	.985
	PPM2C	BG542521	−1.585	.984
	PPP4R2	AI983837	−1.553	.964
Protein folding	DNAJA2	AW057513	−1.543	.943
	DNAJC4	AW071239	1.517	.887
	FLJ14281	AL121021	−1.463	.607
	SEC63	NM_007214	−1.528	.555
Protein modification	MGC10067	H73636	−1.444	.505
Protein phosphorylation	PLK2	NM_006622	−2.783	1.000
	LYN	AI356412	−1.739	.994
	BMP2K	AU145366	−1.577	.980
	MAP4K4	NM_017792	−1.591	.835
	PRKCI	AI689429	−1.574	.781
	ROCK2	AL049383	−1.566	.762
	PRPF4B	Z25435	−1.575	.741
Protein transport	IPO7	AI741392	−1.701	.992
	RANBP5	AU148466	−1.565	.712
Protein ubiquitination	EDD	U69567	−1.640	.946
	FLJ31951	AL553942	−1.601	.944
	FBXW2	AL043967	−1.577	.806
	BAZ1A	NM_013448	−1.575	.774
	PJA2	AA142966	−1.545	.674
	HACE1	AB037741	−1.460	.633
Proton transport	UCP2	U94592	2.045	1.000
Signal transduction	PLK2	NM_006622	−2.783	1.000
	GDF15	AF003934	1.774	.997
	LYN	AI356412	−1.739	.994
	SOCS5	AW664421	−1.678	.993
	IPO7	AI741392	−1.701	.992
	IL7	AW190593	−1.518	.878
	PRKCI	AI689429	−1.574	.781
	ROCK2	AL049383	−1.566	.762
	RAPH1	AA194149	−1.475	.752
	CREBL2	NM_001310	−1.540	.530
	RAPGEF6	AI640834	−1.450	.511
	ARID1A	NM_018450	−1.528	.502
Spermatogenesis	SPANXA1, SPANXA2, SPANXB1, SPANXB2, SPANXC	NM_013453	1.534	.697
Splicing regulation	FUSIP1	AI954700	−1.584	.985
	SR140	AU152088	−1.595	.842
	PRPF4B	Z25435	−1.575	.741
	SFRS6	AL031681	−1.594	.526
Transcription regulation	KLF4	BF514079	2.771	1.000
	SOX18	AFFX-M27830_5	1.945	1.000
	SOX7	AI808807	−2.052	1.000
	BHLHB2	NM_003670	2.051	1.000
	SALL1	AU152837	−1.773	1.000

Table 2. (*continued*)

Function	Gene Symbol	Representative Public ID	Fold Change	Probability
Transcription regulation	ZNF238	AJ223321	−1.883	1.000
	FUSIP1	AI954700	−1.584	.985
	FRBZ1	AW299558	−1.527	.957
	ADNP	BG149849	−1.553	.957
	CHD1	AU155298	−1.516	.952
	TGFB1I4	AK027071	1.695	.942
	SSA2	AU146655	−1.610	.900
	ZBTB11	NM_014415	−1.592	.863
	FOXQ1	AI676059	1.561	.832
	GATA6	D87811	1.559	.775
	BAZ1A	NM_013448	−1.575	.774
	ZNF398	AI950078	−1.471	.713
	NFIB	AI186739	−1.557	.713
	E2F3	NM_001949	−1.553	.712
	ZNF148	NM_021964	−1.539	.630
	JUNB	NM_002229	1.578	.615
	CREBL2	NM_001310	−1.540	.530
	ARID1A	NM_018450	−1.528	.502
	EIF1AX	AL079283	−1.675	.971
Transport	ZNF238	AJ223321	−1.883	1.000
	SLC16A1	AL162079	−1.552	.659

indomethacin treatment in HMECs and breast cancer cells was caused by the increased catabolic breakdown of PtdCho by PLA$_2$ and lysophospholipase and/or the inhibition of GPC phosphodiesterase. Because ^{13}C-labeled Cho was not detected during indomethacin treatment of breast cancer cells in short-term [1,2-^{13}C]choline exposure but was significantly increased following indomethacin treatment in ^{1}H MR spectra, this increase in Cho most likely originated from catabolic processes, such as PLD activation. In long-term experiments, the fractional ^{13}C enrichment in Cho was constant following indomethacin treatment of breast cancer cells, again indicating its catabolic origin. The decrease in total PC and the absence of Cho in the ^{13}C MR spectra of short-term experiments following indomethacin treatment in breast cancer cells suggest that indomethacin also upregulated the anabolic pathway, converting PC to CDP-choline and PtdCho. The smaller total PC pool following indomethacin treatment in breast cancer cells and the reduction in ^{13}C enrichment of this PC pool were most likely a combination of an increased anabolic rate and a faster breakdown of unlabeled PtdCho, causing the dilution of ^{13}C label in the PC pool. These changes were not detected in nonmalignant HMECs. In HMECs, no indomethacin-induced differences were detected in the ^{13}C enrichment of PC in short-term or long-term experiments. In long-term [1,2-^{13}C]-choline exposure experiments, ^{13}C enrichment of PtdCho was significantly increased following indomethacin treatment in HMECs, indicating that indomethacin resulted in an increased anabolic flux of ^{13}C label into membrane PtdCho relative to a constant or decreased catabolic flux of ^{13}C label from PtdCho by phospholipases. However, the absence of an increase in fractional ^{13}C enrichment in GPC in HMECs following indomethacin treatment suggests a contribution to the total GPC increase from an unlabeled pool. In breast cancer cells, this increase of PtdCho ^{13}C enrichment following indomethacin treatment was not observed to the same

extent. In summary, indomethacin appears to cause an increased choline membrane turnover in breast cancer cells by activating multiple phospholipases, as well as the anabolic pathway. In HMECs, indomethacin resulted in an enhanced anabolic pathway, but increased phospholipase activation was not detected following indomethacin treatment.

Microarray analysis of gene expression revealed that mRNA for none of the enzymes directly involved in choline phospholipid metabolism was significantly overexpressed or underexpressed following short-term indomethacin treatment in MCF-12A HMECs and MDA-MB-231 breast cancer cells. In contrast, our earlier study did detect differences in choline phospholipid metabolism−related genes between MCF-12A and MDA-MB-231 cells, explaining in part the significantly different choline metabolite levels in these two cell lines [5]. These data suggest that the changes in choline phospholipid metabolites following indomethacin treatment observed by MRS most likely occurred from changes in enzyme activity rather than from changes in enzyme expression, or indirectly from secondary effects through signaling cascades. However, significant overexpression or underexpression was detected in several genes following 2 hours of indomethacin treatment in MCF-12A HMECs and human MDA-MD-231 breast cancer cells, suggesting that indomethacin causes diverse changes at the transcriptional level. Genes with altered expression following indomethacin treatment were mostly different in the two cell lines. Change in the expression common to both cell lines was observed for only seven genes following the indomethacin treatment of HMECs and breast cancer cells. This may imply mechanistic differences in the actions of indomethacin in HMECs and human breast cancer cells.

The decrease in the mRNA expression of *PTPN12* following indomethacin treatment in MCF-12A HMECs may play a role in causing the changes observed in choline phospholipid metabolism. Protein tyrosine phosphatases are involved

Table 3. Significantly Differentially Expressed Genes Following Indomethacin Treatment in MDA-MB-231 Breast Cancer Cells, by Function.

Function	Gene Symbol	Representative Public ID	Fold Change	Probability
Angiogenesis regulation	RHOB	AI263909	2.032	1.000
	ANGPTL4	NM_016109	2.546	1.000
	IL8	NM_000584	−1.824	.995
Apoptosis regulation	RHOB	AI263909	2.032	1.000
	ANGPTL4	NM_016109	2.546	1.000
	GADD45B	NM_015675	1.640	1.000
	BIRC3	U37546	−1.696	.998
Blood coagulation	SERPINE1	NM_000602	2.067	1.000
	PLAU	NM_002658	1.736	.987
	THBD	NM_000361	−1.509	.506
Cell adhesion	NEDD9	U64317	2.061	1.000
	RHOB	AI263909	2.032	1.000
	IL8	NM_000584	−1.824	.995
Cell cycle regulation	DUSP1	NM_004417	2.856	1.000
	NEDD9	U64317	2.061	1.000
	RHOB	AI263909	2.032	1.000
	SNF1LK	NM_030751	1.834	1.000
	IL8	NM_000584	−1.824	.995
	DUSP6	BC005047	−1.626	.930
	PLK2	NM_006622	−1.550	.738
Cell growth regulation	NEDD9	U64317	2.061	1.000
Cell motility	IL8	NM_000584	−1.824	.995
Chemotaxis	IL8	NM_000584	−1.824	.995
	PLAU	NM_002658	1.736	.987
Choline phospholipid metabolism	JUNB	NM_002229	3.265	1.000
	RHOB	AI263909	2.032	1.000
	EDN1	NM_001955	2.999	1.000
	IL8	NM_000584	−1.824	.995
	CSF2	M11734	1.622	.977
	NGFB	NM_002506	1.610	.966
Cytoskeleton organization	NEDD9	U64317	2.061	1.000
Development	CSF2	M11734	1.622	.977
	NGFB	NM_002506	1.610	.966
	SNAI2	AI572079	1.627	.923
	FZD7	NM_003507	−1.557	.856
	NKX3-1	AF247704	1.514	.577
Differentiation	SNF1LK	NM_030751	1.834	1.000
	GADD45B	NM_015675	1.640	1.000
	IL11	NM_000641	1.515	.504
Endocytosis	TFRC	N76327	−1.770	.909
Endosome-to-lysosome transport	RHOB	AI263909	2.032	1.000
Hypoxia response	ANGPTL4	NM_016109	2.546	1.000
Immune response	GBP1	AW014593	−1.753	.999
	IL6ST	AB015706	−1.642	.778
Ion homeostasis	TFRC	N76327	−1.770	.909
	ATP8B1	BG290908	−1.552	.693
Lipid metabolism	ANGPTL4	NM_016109	2.546	1.000
	NR2F2	AL037401	−1.633	.982
	ATP8B1	BG290908	−1.552	.693
Not determined	AMIGO2	AC004010	2.553	1.000
	VMP1	BF674052	3.353	1.000
	C6orf145	AK024828	1.729	.999
	TXNIP	AA812232	−1.765	.998
	LBH	NM_030915	1.665	.985
	TPD52L1	NM_003287	−1.517	.950
	DKFZP566D1346	AL136717	−1.625	.944
	ZFP36L1	BE620915	1.596	.864
	NET1	NM_005863	1.540	.622
Proliferation regulation	EDN1	NM_001955	2.999	1.000
	IL8	NM_000584	−1.824	.995
	TOB1	BF240286	−1.718	.910
	ADAMTS1	AF060152	−1.726	.898
	KLF4	NM_004235	1.811	.855
	IL11	NM_000641	1.515	.504
Protein dephosphorylation	DUSP6	BC005047	−1.626	.930
	PPM2C	BG542521	−1.574	.735
	DUSP1	AA530892	1.527	.655
Protein phosphorylation	SNF1LK	NM_030751	1.834	1.000
	ARK5	NM_014840	1.668	.988
	PLK2	NM_006622	−1.550	.738
Protein transport	RHOB	AI263909	2.032	1.000
	ARL7	AW450363	−1.651	.991

Table 3. (*continued*)

Function	Gene Symbol	Representative Public ID	Fold Change	Probability
Protein ubiquitination	IBRDC2	AI953847	−1.737	.999
	BIRC3	U37546	−1.696	.998
Proteolysis	PLAU	NM_002658	1.736	.987
	TFRC	N76327	−1.770	.909
	ADAMTS1	AF060152	−1.726	.898
Proton transport	ATP5I	BC003679	1.507	.944
Signal transduction	NEDD9	U64317	2.061	1.000
	TMEPAI	NM_020182	2.653	1.000
	EDN1	NM_001955	2.999	1.000
	SMAD7	NM_005904	1.943	1.000
	BIRC3	U37546	−1.696	.998
	IL8	NM_000584	−1.824	.995
	ARL7	AW450363	−1.651	.991
	PLAU	NM_002658	1.736	.987
	NR2F2	AL037401	−1.633	.982
	CSF2	M11734	1.622	.977
	NGFB	NM_002506	1.610	.966
	ADAMTS1	AF060152	−1.726	.898
	FZD7	NM_003507	−1.557	.856
	IL6ST	AB015706	−1.642	.778
	PLK2	NM_006622	−1.550	.738
	IL11	NM_000641	1.515	.504
Transcription regulation	BHLHB2	BG326045	3.198	1.000
	JUNB	NM_002229	3.265	1.000
	SMAD7	NM_005904	1.943	1.000
	CITED2	NM_006079	−1.799	1.000
	NR2F2	AL037401	−1.633	.982
	SNAI2	AI572079	1.627	.923
	KLF4	NM_004235	1.811	.855
	NKX3-1	AF247704	1.514	.577
	ARID5B	BG285011	−1.496	.518
	JUN	NM_002228	4.347	.514
Transport	SLC19A2	AF153330	1.535	.765

in signaling cascades regulating PtdCho-specific PLC [32] or PtdCho-specific PLD [33]. Protein tyrosine phosphatase inhibition with vanadate induced PC production through PtdCho-specific PLC [32] or PLD [33] activation. Decreased *PTPN12* gene expression could potentially activate PtdCho-specific PLC and PLD. Decreased mRNA expression of *MAP4K4* [34] in MCF-12A HMECs following indomethacin treatment may impact on choline phospholipid metabolism through c-Jun N-terminal kinase [34]. Decreased *PRKCI* expression in MCF-12A HMECs following indomethacin treatment can potentially downregulate group IV cytosolic PLA$_2$ [35] and PtdCho-specific PLD isoform 2 [36]. These effects in gene expression in signaling pathways potentially affecting phospholipases are inconclusive in light of MCF-12A ^{13}C MR data demonstrating no significant activation of phospholipases. The significant decrease in *UGCG* [37] mRNA levels following indomethacin treatment in MCF-12A HMECs can alter choline phospholipid metabolism by increasing the availability of cellular ceramide and sphingomyelin (SM) pools, which may change the SM–PtdCho balance maintained by sphingomyelinase and SM synthase [38]. The actions of sphingomyelinase and SM synthase would also affect cellular PC levels.

In human MDA-MB-231 breast cancer cells, significantly reduced *IL8* expression levels following indomethacin treatment may indicate decreased PtdCho-specific PLD or PLC activity. In cells of the immune system, *IL8* stimulation can elicit increased PtdCho-specific PLD or PLC activity through *IL8* receptors [39]. In bronchial epithelial cells, the activation of PtdCho-specific PLD1 and PLD2 was shown to participate in a signaling cascade, resulting in *IL8* secretion from these cells [40]. Increased *NGFB* polypeptide expression in MDA-MB-231 breast cancer cells treated with indomethacin may be related to the observed increase in choline membrane turnover because nerve growth factor was demonstrated to enhance PtdCho biosynthesis by increasing diacylglycerol cholinephosphotransferase activity [41]. In breast cancer cells, indomethacin-induced *NGFB* expression may have activated PtdCho biosynthesis, which is consistent with our ^{13}C MR data, demonstrating an increased choline membrane turnover in indomethacin-treated breast cancer cells by activating the anabolic pathway. Overexpression of granulocyte–macrophage colony-stimulating factor (*CSF2*) in indomethacin-treated MDA-MB-231 breast cancer cells may be related to the upregulation of PtdCho-specific PLD, as previously demonstrated in human neutrophils [42], consistent with the upregulation of PtdCho-specific phospholipase activity detected in our ^{13}C MRS data. The increased expression of *RHOB* in indomethacin-treated MDA-MB-231 breast cancer cells may be involved in stimulating PtdCho-specific PLD activity, as previously shown [43], consistent with the activation of phospholipases observed in our ^{13}C MRS data. Indomethacin treatment resulted in *EDN1* (or *ET1*) overexpression in human MDA-MB-231 breast

cancer cells. *EDN1* is a potent vasoconstrictor peptide, which can also induce proliferation, differentiation, apoptosis, and matrix metalloprotease expression [44]. In several cell types, such as fibroblasts, myocytes, and osteoblasts, *EDN1*-mediated activation of PtdCho-specific phospholipases D, C, and A$_2$ was demonstrated [45–48]. *EDN1*-evoked PtdCho-PLD and PtdCho-PLA$_2$ activation stimulates the release of arachidonic acid and prostaglandins [47,48]. In breast cancer cells, indomethacin-induced *EDN1* expression most likely activated PtdCho-specific phospholipases, consistent with our ^{13}C MR data, demonstrating the activation of PtdCho-specific phospholipases.

Indomethacin treatment in human MDA-MB-231 breast cancer cells, as well as in MCF-12A HMECs, resulted in the overexpression of *JUNB*, which was more pronounced in the breast cancer cell line. *JUNB* belongs to the *Jun* gene family of the activating protein-1 transcription factors involved in cell growth [49], differentiation [50], cell cycle regulation [51], and, possibly, neoplastic transformation [49]. Overexpression of *JUNB* can repress transcription [52]. *JUNB* transcription can be activated downstream of PtdCho degradation during the G$_1$ phase of the cell cycle [53]. Thus, *JUNB* overexpression may be the result of indomethacin-driven phospholipase activation, which was more pronounced in MDA-MB-231 breast cancer cells than in MCF-12A HMECs, according to ^{13}C MRS data.

Previous studies with MCF-7 breast cancer cells have reported that choline transport is the rate-limiting step in PC synthesis in this breast cancer cell line [7]. Although arachidonic acid has been linked to the activation of the sodium-dependent high-affinity choline transporter [54], the specific molecular choline transporters responsible for the transport of Cho across the plasma membranes of HMECs and human breast cancer cells have not yet been identified. The microarray gene expression analysis performed in our previous study [5] demonstrated that no significant differences in choline transporters were detected between HMECs and breast cancer cells. Indomethacin treatment did not alter gene expression levels in choline transporters in either HMECs or human breast cancer cells. However, it is possible that posttranscriptional changes in choline transporter activities may have been caused by indomethacin treatment.

Indomethacin appears to have multiple effects on the gene expression of human breast cancer cells, some of which may influence PC metabolism indirectly through signaling cascades, such as protein kinases, protein phosphatases, or signaling peptides. Indomethacin-induced *CSF2*, *RHOB*, and *EDN1* overexpression mediating the activation of multiple phospholipases matches well with the ^{13}C data obtained from breast cancer cells; a strong activation of phospholipases was observed with indomethacin treatment in breast cancer cells, but not to the same extent as in HMECs.

In this study, distinct differences were identified for indomethacin-mediated changes in choline metabolite profile in nonmalignant HMECs *versus* breast cancer cells. Indomethacin treatment resulted in an increased choline membrane turnover by activating multiple phospholipases, as well as by enhancing the anabolic pathway in breast cancer cells.

In HMECs, however, indomethacin predominantly increased the rate of anabolic choline membrane metabolism. The changes in choline metabolite profile following indomethacin treatment were not caused by an overexpression or under-expression of the enzymes involved in choline metabolism. The effects of indomethacin treatment on the choline metabolite profile of HMECs and breast cancer cells could well be mediated by a combination of secondary effects or signaling cascades. Microarray analysis of gene expression revealed that indomethacin treatment in HMECs and breast cancer cells caused diverse changes at the transcriptional level, which were mostly nonuniform for HMECs and breast cancer cells. This may imply mechanistic differences in the effects of indomethacin treatment on HMECs *versus* breast cancer cells. Candidate genes mediating the indomethacin-induced changes in choline phospholipid metabolism include *IL8*, *NGFB*, *CSF2*, *RHOB*, *EDN1*, and *JUNB* in breast cancer cells. The characteristic changes in choline membrane metabolism during indomethacin treatment observed here support further investigation of the role of NSAIDs in cancer prevention and in the treatment of primary and metastatic diseases. The application of ^{13}C MR spectroscopy, combined with microarray gene expression analysis, was shown to be a useful tool in characterizing distinct mechanisms of such NSAID treatment in human breast cancer.

References

[1] Leach MO, Verrill M, Glaholm J, Smith TA, Collins DJ, Payne GS, Sharp JC, Ronen SM, McCready VR, Powles TJ, et al. (1998). Measurements of human breast cancer using magnetic resonance spectroscopy: a review of clinical measurements and a report of localized ^{31}P measurements of response to treatment. *NMR Biomed* **11**, 314–340.

[2] Ruiz-Cabello J and Cohen JS (1992). Phospholipid metabolites as indicators of cancer cell function. *NMR Biomed* **5**, 226–233.

[3] Aboagye EO and Bhujwalla ZM (1999). Malignant transformation alters membrane choline phospholipid metabolism of human mammary epithelial cells. *Cancer Res* **59**, 80–84.

[4] Ramirez de Molina A, Gutierrez R, Ramos MA, Silva JM, Silva J, Bonilla F, Sanchez JJ, and Lacal JC (2002). Increased choline kinase activity in human breast carcinomas: clinical evidence for a potential novel antitumor strategy. *Oncogene* **21**, 4317–4322.

[5] Glunde K, Jie C, and Bhujwalla ZM (2004). Molecular causes of the aberrant choline phospholipid metabolism in breast cancer. *Cancer Res* **64**, 4270–4276.

[6] Noh DY, Ahn SJ, Lee RA, Park IA, Kim JH, Suh PG, Ryu SH, Lee KH, and Han JS (2000). Overexpression of phospholipase D1 in human breast cancer tissues. *Cancer Lett* **161**, 207–214.

[7] Katz-Brull R and Degani H (1996). Kinetics of choline transport and phosphorylation in human breast cancer cells; NMR application of the zero trans method. *Anticancer Res* **16**, 1375–1380.

[8] Bhujwalla ZM, Aboagye EO, Gillies RJ, Chacko VP, Mendola CE, and Backer JM (1999). Nm23-transfected MDA-MB-435 human breast carcinoma cells form tumors with altered phospholipid metabolism and pH: a ^{31}P nuclear magnetic resonance study *in vivo* and *in vitro*. *Magn Reson Med* **41**, 897–903.

[9] Ronen SM, Jackson LE, Beloueche M, and Leach MO (2001). Magnetic resonance detects changes in phosphocholine associated with Ras activation and inhibition in NIH 3T3 cells. *Br J Cancer* **84**, 691–696.

[10] Sterin M, Cohen JS, Mardor Y, Berman E, and Ringel I (2001). Levels of phospholipid metabolites in breast cancer cells treated with antimitotic drugs: a (31)P-magnetic resonance spectroscopy study. *Cancer Res* **61,** 7536–7543.

[11] Natarajan K, Mori N, Artemov D, and Bhujwalla ZM (2002). Exposure of human breast cancer cells to the anti-inflammatory agent indomethacin alters choline phospholipid metabolites and Nm23 expression. *Neoplasia* **4,** 409–416.

[12] Glunde K, Ackerstaff E, Natarajan K, Artemov D, and Bhujwalla ZM (2002). Real-time changes in ^{1}H and ^{31}P NMR spectra of malignant human mammary epithelial cells during treatment with the anti-inflammatory agent indomethacin. *Magn Reson Med* **48,** 819–825.

[13] Narayana PA (2005). Magnetic resonance spectroscopy in the monitoring of multiple sclerosis. *J Neuroimaging* **15,** 46S–57S.

[14] Johnsen JI, Lindskog M, Ponthan F, Pettersen I, Elfman L, Orrego A, Sveinbjornsson B, and Kogner P (2005). NSAIDs in neuroblastoma therapy. *Cancer Lett* **228,** 195–201.

[15] Rome LH and Lands WE (1975). Structural requirements for time-dependent inhibition of prostaglandin biosynthesis by anti-inflammatory drugs. *Proc Natl Acad Sci USA* **72,** 4863–4865.

[16] Connolly JM, Liu XH, and Rose DP (1996). Dietary linoleic acid–stimulated human breast cancer cell growth and metastasis in nude mice and their suppression by indomethacin, a cyclooxygenase inhibitor. *Nutr Cancer* **25,** 231–240.

[17] Gately S (2000). The contributions of cyclooxygenase-2 to tumor angiogenesis. *Cancer Metastasis Rev* **19,** 19–27.

[18] Jones MK, Wang H, Peskar BM, Levin E, Itani RM, Sarfeh IJ, and Tarnawski AS (1999). Inhibition of angiogenesis by nonsteroidal anti-inflammatory drugs: insight into mechanisms and implications for cancer growth and ulcer healing. *Nat Med* **5,** 1418–1423.

[19] Vane JR and Botting RM (1998). Mechanism of action of antiinflammatory drugs. *Int J Tissue React* **20,** 3–15.

[20] Lupulescu A (1996). Prostaglandins, their inhibitors and cancer. *Prostaglandins Leukot Essent Fat Acids* **54,** 83–94.

[21] Marks F, Muller-Decker K, and Furstenberger G (2000). A causal relationship between unscheduled eicosanoid signaling and tumor development: cancer chemoprevention by inhibitors of arachidonic acid metabolism. *Toxicology* **153,** 11–26.

[22] Ronen SM and Degani H (1992). The application of ^{13}C NMR to the characterization of phospholipid metabolism in cells. *Magn Reson Med* **25,** 384–389.

[23] Paine TM, Soule HD, Pauley RJ, and Dawson PJ (1992). Characterization of epithelial phenotypes in mortal and immortal human breast cells. *Int J Cancer* **50,** 463–473.

[24] Tyagi RK, Azrad A, Degani H, and Salomon Y (1996). Simultaneous extraction of cellular lipids and water-soluble metabolites: evaluation by NMR spectroscopy. *Magn Reson Med* **35,** 194–200.

[25] Irizarry RA, Hobbs B, Collin F, Beazer-Barclay YD, Antonellis KJ, Scherf U, and Speed TP (2003). Exploration, normalization, and summaries of high density oligonucleotide array probe level data. *Biostatistics* **4,** 249–264.

[26] Bolstad BM, Irizarry RA, Astrand M, and Speed TP (2003). A comparison of normalization methods for high density oligonucleotide array data based on variance and bias. *Bioinformatics* **19,** 185–193.

[27] Newton MA and Kendziorski CM (2003). Parametric empirical Bayes methods for microarrays. In *The Analysis of Gene Expression Data: Methods and Software.* Parmigiani G, Garrett ES, Irizarry R, Zeger SL, Parmigiani G, Garrett ES, Irizarry R, and Zeger SL (Eds). Springer-Verlag, New York.

[28] Howe LR, Subbaramaiah K, Brown AM, and Dannenberg AJ (2001). Cyclooxygenase-2: a target for the prevention and treatment of breast cancer. *Endocr-Relat Cancer* **8,** 97–114.

[29] O'Byrne KJ, Dalgleish AG, Browning MJ, Steward WP, and Harris AL (2000). The relationship between angiogenesis and the immune response in carcinogenesis and the progression of malignant disease. *Eur J Cancer* **36,** 151–169.

[30] Cao Y, Pearman AT, Zimmerman GA, McIntyre TM, and Prescott SM (2000). Intracellular unesterified arachidonic acid signals apoptosis. *Proc Natl Acad Sci USA* **97,** 11280–11285.

[31] Yeung DK, Cheung HS, and Tse GM (2001). Human breast lesions: characterization with contrast-enhanced *in vivo* proton MR spectroscopy—initial results. *Radiology* **220,** 40–46.

[32] Sakai T, Sugiyama T, Banno Y, Kato Y, and Nozawa Y (2004). Involvement of phosphatidylcholine hydrolysis by phospholipase C in prostaglandin F2alpha–induced 1,2-diacylglycerol formation in osteoblast-like MC3T3-E1 cells. *J Bone Miner Metab* **22,** 198–206.

[33] Koike T, Mizutani T, Hirai K, Morita Y, and Nozawa Y (1993). SCF/c-kit receptor–mediated arachidonic acid liberation in rat mast cells. Involvement of PLD activation associated tyrosine phosphorylation. *Biochem Biophys Res Commun* **197,** 1570–1577.

[34] Machida N, Umikawa M, Takei K, Sakima N, Myagmar BE, Taira K, Uezato H, Ogawa Y, and Kariya K (2004). Mitogen-activated protein kinase kinase kinase kinase 4 as a putative effector of Rap2 to activate the c-Jun N-terminal kinase. *J Biol Chem* **279,** 15711–15714.

[35] Anthonsen MW, Andersen S, Solhaug A, and Johansen B (2001). Atypical lambda/iota PKC conveys 5-lipoxygenase/leukotriene B4–mediated cross-talk between phospholipase A$_2$s regulating NF-kappa B activation in response to tumor necrosis factor-alpha and interleukin-1beta. *J Biol Chem* **276,** 35344–35351.

[36] Mwanjewe J, Spitaler M, Ebner M, Windegger M, Geiger M, Kampfer S, Hofmann J, Uberall F, and Grunicke HH (2001). Regulation of phospholipase D isoenzymes by transforming Ras and atypical protein kinase C-iota. *Biochem J* **359,** 211–217.

[37] Yamashita T, Wada R, Sasaki T, Deng C, Bierfreund U, Sandhoff K, and Proia RL (1999). A vital role for glycosphingolipid synthesis during development and differentiation. *Proc Natl Acad Sci USA* **96,** 9142–9147.

[38] Pettus BJ, Chalfant CE, and Hannun YA (2002). Ceramide in apoptosis: an overview and current perspectives. *Biochim Biophys Acta* **1585,** 114–125.

[39] Bacon KB, Flores-Romo L, Life PF, Taub DD, Premack BA, Arkinstall SJ, Wells TN, Schall TJ, and Power CA (1995). IL-8–induced signal transduction in T lymphocytes involves receptor-mediated activation of phospholipases C and D. *J Immunol* **154,** 3654–3666.

[40] Wang L, Cummings R, Usatyuk P, Morris A, Irani K, and Natarajan V (2002). Involvement of phospholipases D1 and D2 in sphingosine 1-phosphate–induced ERK (extracellular-signal–regulated kinase) activation and interleukin-8 secretion in human bronchial epithelial cells. *Biochem J* **367,** 751–760.

[41] Araki W and Wurtman RJ (1997). Control of membrane phosphatidylcholine biosynthesis by diacylglycerol levels in neuronal cells undergoing neurite outgrowth. *Proc Natl Acad Sci USA* **94,** 11946–11950.

[42] Bourgoin S, Plante E, Gaudry M, Naccache PH, Borgeat P, and Poubelle PE (1990). Involvement of a phospholipase D in the mechanism of action of granulocyte–macrophage colony-stimulating factor (GM-CSF): priming of human neutrophils *in vitro* with GM-CSF is associated with accumulation of phosphatidic acid and diacylglycerol. *J Exp Med* **172,** 767–777.

[43] Exton JH (2000). Phospholipase D. *Ann N Y Acad Sci* **905,** 61–68.

[44] Grant K, Loizidou M, and Taylor I (2003). Endothelin-1: a multifunctional molecule in cancer. *Br J Cancer* **88,** 163–166.

[45] Pai JK, Dobek EA, and Bishop WR (1991). Endothelin-1 activates phospholipase D and thymidine incorporation in fibroblasts overexpressing protein kinase C beta 1. *Cell Regul* **2,** 897–903.

[46] Clerk A and Sugden PH (1997). Regulation of phospholipases C and D in rat ventricular myocytes: stimulation by endothelin-1, bradykinin and phenylephrine. *J Mol Cell Cardiol* **29,** 1593–1604.

[47] Kozawa O, Suzuki A, Shinoda J, Ozaki N, Oiso Y, and Uematsu T (1997). Involvement of phospholipase D activation in endothelin-1–induced release of arachidonic acid in osteoblast-like cells. *J Cell Biochem* **64,** 376–381.

[48] Yousufzai SY and Abdel-latif AA (1997). Endothelin-1 stimulates the release of arachidonic acid and prostaglandins in cultured human ciliary muscle cells: activation of phospholipase A$_2$. *Exp Eye Res* **65,** 73–81.

[49] Mathas S, Hinz M, Anagnostopoulos I, Krappmann D, Lietz A, Jundt F, Bommert K, Mechta-Grigoriou F, Stein H, Dorken B, et al. (2002). Aberrantly expressed c-Jun and JunB are a hallmark of Hodgkin lymphoma cells, stimulate proliferation and synergize with NF-kappa B. *EMBO J* **21,** 4104–4113.

[50] Jacobs-Helber SM, Abutin RM, Tian C, Bondurant M, Wickrema A, and Sawyer ST (2002). Role of JunB in erythroid differentiation. *J Biol Chem* **277,** 4859–4866.

[51] Bakiri L, Lallemand D, Bossy-Wetzel E, and Yaniv M (2000). Cell cycle–dependent variations in c-Jun and JunB phosphorylation: a role in the control of cyclin D1 expression. *EMBO J* **19,** 2056–2068.

[52] Shaulian E and Karin M (2002). AP-1 as a regulator of cell life and death. *Nat Cell Biol* **4,** E131–E136.

[53] Jackowski S, Xu XX, and Rock CO (1997). Phosphatidylcholine signaling in response to CSF-1. *Mol Reprod Dev* **46,** 24–30.

[54] Saltarelli MD, Yamada K, and Coyle JT (1990). Phospholipase A$_2$ and ^{3}H-hemicholinium-3 binding sites in rat brain: a potential second-messenger role for fatty acids in the regulation of high-affinity choline uptake. *J Neurosci* **10,** 62–72.